Yamauchi *et al. Cancer & Metabolism* (2024) 12:23
https://doi.org/10.1186/s40170-024-00352-4

Cancer & Metabolism

RESEARCH Open Access

Epigenetic repression of de novo cysteine synthetases induces intra-cellular accumulation of cysteine in hepatocarcinoma by up-regulating the cystine uptake transporter xCT

Tomoaki Yamauchi[1], Yumi Okano[1], Daishu Terada[1], Sai Yasukochi[1], Akito Tsuruta[1], Yuya Tsurudome[3], Kentaro Ushijima[3], Naoya Matsunaga[2], Satoru Koyanagi[1*] and Shigehiro Ohdo[1*]

Abstract

Background The metabolic reprogramming of amino acids is critical for cancer cell growth and survival. Notably, intracellular accumulation of cysteine is often observed in various cancers, suggesting its potential role in alleviating the oxidative stress associated with rapid proliferation. The liver is the primary organ for cysteine biosynthesis, but much remains unknown about the metabolic alterations of cysteine and their mechanisms in hepatocellular carcinoma cells.

Methods RNA-seq data from patients with hepatocarcinoma were analyzed using the TNMplot database. The underlying mechanism of the oncogenic alteration of cysteine metabolism was studied in mice implanted with BNL 1ME A.7 R.1 hepatocarcinoma.

Results Database analysis of patients with hepatocellular carcinoma revealed that the expression of enzymes involved in de novo cysteine synthesis was down-regulated accompanying with increased expression of the cystine uptake transporter xCT. Similar alterations in gene expression have also been observed in a syngeneic mouse model of hepatocarcinoma. The enhanced expression of DNA methyltransferase in murine hepatocarcinoma cells caused methylation of the upstream regions of cysteine synthesis genes, thereby repressing their expression. Conversely, suppression of de novo cysteine synthesis in healthy liver cells induced xCT expression by up-regulating the oxidative-stress response factor NRF2, indicating that reduced de novo cysteine synthesis repulsively increases cystine uptake via enhanced xCT expression, leading to intracellular cysteine accumulation. Furthermore, the pharmacological inhibition of xCT activity decreased intracellular cysteine levels and suppressed hepatocarcinoma tumor growth in mice.

*Correspondence:
Satoru Koyanagi
koyanagi@phar.kyushu-u.ac.jp
Shigehiro Ohdo
ohdo@phar.kyushu-u.ac.jp

Full list of author information is available at the end of the article

© The Author(s) 2024. **Open Access** This article is licensed under a Creative Commons Attribution-NonCommercial-NoDerivatives 4.0 International License, which permits any non-commercial use, sharing, distribution and reproduction in any medium or format, as long as you give appropriate credit to the original author(s) and the source, provide a link to the Creative Commons licence, and indicate if you modified the licensed material. You do not have permission under this licence to share adapted material derived from this article or parts of it.The images or other third party material in this article are included in the article's Creative Commons licence, unless indicated otherwise in a credit line to the material. If material is not included in the article's Creative Commons licence and your intended use is not permitted by statutory regulation or exceeds the permitted use, you will need to obtain permission directly from the copyright holder.To view a copy of this licence, visit http://creativecommons.org/licenses/by-nc-nd/4.0/.

Conclusions Our findings indicate an underlying mechanism of the oncogenic alteration of cysteine metabolism in hepatocarcinoma and highlight the efficacy of alteration of cysteine metabolism as a viable therapeutic target in cancer.

Keywords Cysteine metabolism, xCT, de novo cysteine synthesis, Hepatocarcinoma, DNA methylation, NRF2, Erastin

Background

Oncogenic transformation is accompanied by alterations in cellular metabolism to provide energy and a variety of substrates that enable the rapid proliferation and survival of cancer cells [1, 2]. Amino acids serve not only as essential precursors for protein synthesis but also as regulators of gene expression and as cell signaling molecules. Therefore, an optimal balance of amino acid metabolism is crucial for health. Abnormal changes in amino acid metabolism are often observed in malignant cancers, which play an important role in maintaining rapid tumor growth and survival against various stresses such as oxidative damage, energy deprivation, and chemotherapeutic agents [3, 4]; thus, metabolic reprogramming of amino acids is emerging as a therapeutic target for the treatment of cancer [5].

Cysteine serves as the sulfur source for various biomolecules and plays a critical role in protein synthesis, redox homeostasis, cell signaling, and detoxification [6, 7]. Intracellular cysteine is synthesized from methionine through a trans-sulfuration pathway or taken up from the extracellular environment in the form of cystine through the cystine/glutamate antiporter xCT, encoded by the *SLC7A11* gene [8]. Intracellular accumulation of cysteine has been detected in glioblastoma, triple-negative breast cancer, and non-small cell lung cancer [9–11], suggesting its potential role in alleviating the oxidative stress associated with rapid cell proliferation and/or exposure to chemotherapeutic agents. Despite a decrease in de novo synthesis, xCT expression is up-regulated in those tumor cells. These alterations in cysteine metabolism are characteristic features of cancer cells and are anticipated to be potential therapeutic targets. The liver is the main organ responsible for regulation of cysteine homeostasis [12, 13]. Although previous report indicates oncogenic alteration of cysteine metabolism in hepatic cancer cells [14], our understanding about the mechanism is limited.

BNL 1ME A.7 R.1 cells are a murine hepatocarcinoma cell line generated by treating BALB/c mice-derived hepatocytes with methylcholanthrene epoxide [15, 16]. In this study, we used BNL 1ME A.7 R.1 cells to prepare a syngeneic implantation mouse model of hepatocarcinoma. These hepatocarcinoma animal models showed intra-tumoral accumulation of cysteine and altered gene expression involved in cysteine metabolism, as observed in patients with hepatocellular carcinoma. Namely, the expression of enzymes involved in de novo cysteine synthesis was down-regulated in hepatocarcinoma cells, accompanied by increased expression of the cystine uptake transporter xCT; thus, we employed this animal model to investigate the underlying mechanism of the oncogenic alteration of cysteine. Our findings reveal a novel mechanism for the metabolic alteration of cysteine in oncogenic transformed cells and provide further support for the efficacy of xCT as a therapeutic target for the treatment of malignant cancers.

Methods

Database analysis of gene expression profiles in patients with liver hepatocellular carcinoma

The expression levels of *cystathionine-β-synthase (CBS)*, *cystathionine-γ-lyase (CTH)*, and *SLC7A11* (encoding xCT) in normal tissues and tumors of patients were analyzed using the TNMplot database (https://tnmplot.com/analysis/) [17]. The gene expression levels of *CBS*, *CTH*, and *SLC7A11* in the liver hepatocellular carcinoma (LIHC), based on the tumor grade in The Cancer Genome Atlas (TCGA), were analyzed using the University of Alabama Cancer database (https://ualcan.path.uab.edu/index.html) [18].

The prognostic significance of *CBS*, *CTH*, and *SLC7A11* expression in LIHC patients was analyzed using the Kaplan–Meier plotter database (http://kmplot.com/analysis/) [19]. The method to set a cut-off value and assign the samples to one of two cohorts (high expression or low expression) are described previous reports written by Lánczky & Győrffy [20]. Briefly, they predefine the number of quartiles in the sample and calculate the P-value using COX regression analysis for each cutoff value set at a number between the first and third quartiles. Then, the most significant cutoff value is used as the best cutoff value to separate the input data into two groups.

Cell culture and treatment

BNL 1ME A.7 R.1 cells (RRID: CVCL_6371), a murine hepatic cancer cell line, were purchased from the American Type Culture Collection (Manassas, VA). HepG2 cells were supplied by the Cell Resource Center for Biomedical Research, Tohoku University (Sendai, Japan). The cells were incubated in Dulbecco's modified Eagle's medium (DMEM; Sigma-Aldrich, St. Louis, MO). The medium was supplemented with 5% Fetal Bovine Serum (FBS; Biowest, Nuaillé, France) and 0.25% penicillin-streptomycin (Thermo Fisher Scientific, Waltham, MA). HepaRG cells (KAC, Kyoto, Japan) were grown according to the manufacturer's instructions. Briefly, the cells

were seeded in culture dishes and maintained in growth medium (William's E medium) supplemented with 10% FBS, 0.25% penicillin-streptomycin, 5 μg/mL insulin, 2 mM glutamine, and 50 μM hydrocortisone hemisuccinate. The cells were maintained at 37 °C in a humidified 5% CO_2 atmosphere. The absence of microbes in these cell lines was confirmed using a MycoBlue Mycoplasma Detector (Nanjing Vazyme Biotech, Nanjing, China). Cell lines were authenticated by each cell bank using short tandem repeat-PCR analysis, and these cell lines were used within six months from frozen stocks. Cells were seeded in culture plates and cultured in standard medium (DMEM containing 5% FBS and 0.25% penicillin-streptomycin) for 24 h. After confirmation of attachment, cells were treated with erastin (Cayman Chemical, Ann Arbor, MI), decitabine (Tokyo Chemical Industry), aminooxy acetic acid (AOAA; Fujifilm Wako Pure Chemical), propargylglycine (PAG; Sigma-Aldrich), Akt inhibitor X (Akti X; Cayman Chemical), or 4-octyl itaconate (4-OI; Tokyo Chemical Industry). As a vehicle control, the cells were treated with 0.5% (v/v) DMSO.

Cystine-containing and cystine-deficient media were prepared from Gibco DMEM with high glucose, but without glutamine, methionine, or cystine (#21013-024; Thermo Fisher Scientific) supplemented with 1 mM L-sodium pyruvate (Nacalai Tesque, Kyoto, Japan), 5% FBS, and 0.25% penicillin-streptomycin. L-methionine (Fujifilm Wako Pure Chemical Co., Tokyo, Japan) and L-glutamine (Tokyo Chemical Industry, Tokyo, Japan) were added to the media at final concentrations of 200 μM and 4 mM, respectively. To prepare cysteine-containing media, L-cystine dihydrochloride (Fujifilm Wako Pure Chemical) was added at a final concentration of 200 μM. Cells were seeded in culture plates and cultured in standard medium (DMEM containing 5% FBS and 0.25% penicillin-streptomycin) for 24 h. After the confirmation of cell attachment, the standard media were replaced with cystine-containing media or cystine-deficient media.

Construction of *Slc7a11*-, *Dnmt1*-, *Dnmt3a*-, *Dnmt3b*, or *Nrf2*-knockdown (KD) hepatocarcinoma cells

Small hairpin RNA (shRNA) expressing vectors against the mouse *Slc7a11*, *Dnmt1*, *Dnmt3a*, or *Dnmt3b* gene were purchased from VectorBuilder (Chicago, IL). Lentivirus particles were prepared by the Lentiviral High Titer Packaging Mix with pLVSIN series (Clontech, Palo Alto, CA) using Lenti-X 293 T-cell lines. shRNA-expressing lentivirus particles and 10 μg/mL of polybrene were added to the medium of BNL 1ME A.7 R.1 cells, and then incubated for 24 h. To select clones stably expressing shRNA, cells were maintained in a medium containing 5 μg/mL of puromycin (Fujifilm Wako Pure Chemical). Small interfering RNA (siRNA) against the mouse *Nrf2* gene were purchased from Merck (Darmstadt, Germany). The siRNA was transfected into BNL 1ME A.7 R.1 cells using Lipofectamine 2000 (Thermo Fisher Scientific). Down-regulation of each gene was confirmed by western blotting. To construct control cells, BNL 1ME A.7 R.1 cells were infected with lentivirus particles derived from the shScramble vector and were cultured in puromycin-containing medium, as described above, to select the stably expressing cells.

Animals and treatments

We housed 6–8 male BALB/c mice per cage, with each cage being 30 cm × 40 cm × 16 cm, providing enough space. They were kept under a standardized light-dark cycle at 24±1 °C, humidity at 60±10% and food and water provided *ad libitum*. BNL 1ME A.7 R.1 cells (1×10^6 cells) suspended in 50 μL of PBS were implanted subcutaneously into the back of male BALB/c mice. Tumors were measured using a caliper, and the volume was calculated using the formula of an ellipsoid [tumor volume (mm^3) = π/6 (d1 × d2 × d3), where d1, d2, and d3 represent the three diameters]. After confirming the tumor formation, drug administration was initiated. BNL 1ME A.7 R.1 cell-implanted mice were intraperitoneally injected with erastin (30 mg/kg body weight) or vehicle (10% dimethyl sulfoxide and 50% polyethylene glycol in saline) for every three days. Tumor volume was also measured every three days. All protocols involving mice were reviewed and approved by the Animal Care and Use Committee of Kyushu University (A22-329-1). All methods were performed according to the relevant guidelines and regulations.

Hepatocyte isolation and primary cell culture

Hepatocytes were isolated from male BALB/c mice using the collagenase perfusion method [21, 22]. Cells were plated in 6-well or 24-well plates at a density of 4×10^6 or 8×10^5 cells per well in Williams' medium (Sigma-Aldrich) containing 5% FBS, 0.1 μM insulin (Fujifilm Wako Pure Chemical), 0.1 μM dexamethasone (Fujifilm Wako Pure Chemical), and 1% penicillin/streptomycin and incubated at 37 °C, in a humidified 5% CO_2 atmosphere. After confirming cell attachment, the cells were used in each experiment.

Cell viability assay

The cells were seeded at a density of 1000 cells / well in 96-well plates. After incubation for 24 h, the medium was exchanged with cystine-containing medium or cystine-deficient medium. For the inhibition of xCT activity, cells were treated with 1.5 μM erastin or 0.5% (v/v) DMSO in standard medium. Cell viability was assessed at the indicated time points using the CellTiter-Glo Luminescent Cell Viability Assay System (Promega, Madison, WI)

following the manufacturer's instrument. Chemiluminescence was measured using an EnSpire Multimode Plate Reader (PerkinElmer Japan, Kanagawa, Japan).

Measurement of the intracellular metabolite levels

Cysteine-related metabolites and coenzyme A in the liver, BNL 1ME A.7 R.1-formed tumors in mice, and cultured cells were extracted using the Bligh–Dyer method. To prepare tissue samples, 100 mg of tissue was homogenized with saline and then centrifuged at 12,000 × g for 10 min at 4 °C. Next, 100 µL of homogenates were deproteinized by mixing an equal amount of 5% (w/v) 5-sulfosalicylic acid containing internal standard (2 mg/mL L-[1-^{13} C] valine) and centrifuging at 12,000 × g for 10 min at 4 °C. Then, 150 µL of supernatants were mixed with 150 µL of chloroform and 300 µL of methanol. To prepare cell samples, cells were washed with saline, and homogenized with 300 µL of methanol containing 5 µL of internal standard (10 µg/mL L-[1-^{13} C] valine). The homogenates were centrifuged at 12,000 × g for 10 min at 4 °C. Next, 100 µL of chloroform and 200 µL of supernatants were mixed with 5% (w/v) 5-sulfosalicylic acid. After 10 min of incubation at room temperature, samples were mixed with chloroform (150 µL for tissues, 100 µL for cells) and water (150 µL for tissues, 100 µL for cells). The samples were centrifuged at 1,500 × g for 10 min at 4 °C, and the upper phase were dried out and then dissolved into 50 µL of the mobile phase. A liquid chromatography-tandem mass spectrometry system (Waters, Milford, MA) was used to quantify cysteine-related metabolites. For measurement of amino acids, liquid chromatography was performed using an Intrada amino acid column (3 µm, 50 mm × 3 mm; Imtakt Co., Kyoto, Japan) under a gradient elution program. The mobile phase consisted of solvent A (acetonitrile: tetrahydrofuran:25 mM ammonium formate: formic acid = 9:75:16:0.3, v/v/v/v) and solvent B (acetonitrile:100 mM ammonium formate = 1:4, v/v). The following gradient program was applied: 2.5 min isocratic at 100% buffer A, 4 min gradient to 17% buffer B, 3.5 min isocratic at 100% buffer B, and 5 min isocratic at 100% buffer A with a flow rate of 0.6 mL/min. The mass spectrometer was operated in the multiple reaction monitoring (MRM) mode using positive electrospray ionization. In MRM, the mass-to-charge ratios (m/z) were 241 − 152, 122 − 76.1, 136 − 90, 223 − 134, 149.9-133.1, 399.2-250.1, and 119 − 72 for cystine, cysteine, homocysteine, cystathionine, methionine, *S*-adenosylmethionine, and L-[1-^{13} C] valine, respectively. For measurement of coenzyme A, liquid chromatography was performed using an CORTECS C18 + column (2.7 µm, 100 mm × 2.1 mm; Waters) under a gradient elution program. The mobile phase consisted of solvent A (5 mM ammonium acetate) and solvent B (acetonitrile). The following gradient program was applied: 6 min gradient from 97% buffer A to 95% buffer B, 1 min isocratic at 95% buffer B, 0.5 min gradient to 97% buffer A, and 2.5 min isocratic at 97% buffer A with a flow rate of 0.25 mL/min. The mass spectrometer was operated in the MRM mode using positive electrospray ionization. In MRM, the mass-to-charge ratios (m/z) were 768 − 261 for coenzyme A. The metabolite levels were normalized to the protein concentrations measured using the Pierce BCA Assay Kit (Thermo Fisher Scientific).

Measurement of the intracellular contents of GSH

The collected tissues were homogenized in 40 µL of 5% 5-sulfosalicylic acid. The homogenates were centrifuged at 12,000 × g for 10 min at 4 °C, and the supernatants were collected. GSH concentration was measured using the GSSG/GSH Quantification Kit (Dojindo, Kumamoto, Japan) following the manufacturer's instructions and normalized to tissue weight.

Cystine uptake assay

Hepatocytes were isolated from BNL 1ME A.7 R.1 tumor-bearing mice using the collagenase perfusion method. BNL 1ME A.7 R.1-formed tumors in mice were isolated from the same mice. The isolated tumors were minced and incubated in DMEM containing 1 mg/mL collagenase at 37 °C for 1 h. After quenching collagenase using DMEM containing 5% FBS, tumor cells were dissociated into single cells passing through a cell strainer and then centrifuged at 300 × g for 5 min at 4 °C. Cells were hemolyzed by mixing with ACK buffer (150 mM NH_4Cl, 10 mM $KHCO_3$, and 0.001 mM EDTA-2Na-$2H_2O$) and centrifuging at 300 × g for 5 min at 4 °C. Cells were incubated in Krebs-Ringer buffer (11.7 mM NaCl, 4.7 mM KCl, 1.2 mM $MgCl_2$, 1.2mM NaH_2PO_4-$2H_2O$, 10 mM HEPES, 2.5 mM $CaCl_2$, and 11 mM D-(+)-glucose (pH7.4)) containing 0.5 µCi/mL L-[1-^{14} C] cystine (PerkinElmer Japan) at 37 °C. At the indicated times, cells were washed four times with 1 mL of ice-cold PBS and homogenized with 10% NaOH solution. After centrifugation, the supernatant was used for scintillation counting and protein concentration measurements. Radioactivity was normalized to protein concentrations.

DNA methylation analysis

Genomic DNA was extracted from the tissues using the Wizard Genomic DNA Purification Kit (Promega) according to the manufacturer's instructions. First, 500 ng of DNA was used for the bisulfite reaction using an EZ DNA Methylation Kit (Zymo Research, Irvine, CA). Bisulfite-converted DNA was amplified using the GoTaq Green Master Mix (Promega). Primers were designed using MethPrimer (https://www.urogene.org/cgi-bin/methprimer/methprimer.cgi), and the primer sequences are listed in Supplementary Table S1.

Isolation of membrane and nuclear fraction

Membrane fractions from mouse livers and BNL 1ME A.7 R.1 cell-formed tumors in mice were prepared by ultracentrifugation. The tissues were homogenized in Krebs-Ringer buffer (11.7 mM NaCl, 4.7 mM KCl, 1.2 mM $MgCl_2$, 1.2 mM NaH_2PO_4-$2H_2O$, 25 mM $NaHCO_3$, 2.5 mM $CaCl_2$-$2H_2O$, and 11 mM d-(+)-glucose) containing protease inhibitors (1 μg/mL leupeptin, 1 μg/mL aprotinin, and 100 μM phenylmethanesulfonyl fluoride). Lysates were then separated by centrifugation at 8,000 × g for 15 min at 4 °C, and the supernatants were centrifuged at 100,000 × g for 1 h at 4 °C. Pellets were resuspended in MOPS-Tris buffer (20 mM 4-morpholine propanesulfonic acid–Tris (pH 7.0), 300 mM sucrose, 5 mM EDTA, and protease inhibitors) and ultracentrifuged at 100,000 × g for 1 h at 4 °C. The pellets were resuspended in Tris-EDTA buffer (10 mM Tris-HCl; pH 7.0, 5 mM EDTA, and protease inhibitors). Membrane fractions were prepared from cultured cells using the Fraction-PREP Cell Fractionation Kit (Abcam, Cambridge, UK) according to the manufacturer's instructions. Preparation of nuclear fractions from mouse liver, BNL 1ME A.7 R.1-formed tumors in mice, and cultured cells was conducted using a LysoPure Nuclear and Cytoplasmic Extractor Kit (Fujifilm Wako Pure Chemical) according to the manufacturer's instructions.

Western blotting

Total protein from cells and tissues was prepared using CelLytic MT (Sigma-Aldrich) according to the manufacturer's instructions. Proteins of the plasma membranes and nuclei were prepared using the following methods. Denatured samples were separated by sodium dodecyl sulfate-polyacrylamide gel electrophoresis (SDS-PAGE) and transferred onto polyvinylidene difluoride membranes. The membranes were incubated with primary antibodies against CBS (14787-1-AP, Proteintech, Wuhan, China, RRID: AB_2070970), CTH (12217-1-AP, Proteintech, AB_2087497), xCT (#98051, Cell Signaling Technology, Danvers, MA, RRID: AB_2800296), glutamate-cysteine ligase catalytic subunit (GCLC; sc-390811, Santa Cruz Biotechnology, Santa Cruz, CA, RRID: AB_2736837), glutamate-cysteine ligase modifier subunit (GCLM; sc-55586, Santa Cruz Biotechnology, RRID: AB_831789), DNA (cytosine-5)-methyltransferase 1 (DNMT1; #5032, Cell Signaling Technology, RRID: AB_10548197), DNMT3A (20954-1-AP, Proteintech, RRID: AB_10733339), DNMT3B (26971-1-AP, Proteintech, RRID: AB_2880705), activating transcription factor-4 (ATF4; sc-200, Santa Cruz Biotechnology, RRID: AB_2058752), NF-E2-related factor 2 (NRF2; 16396-1-AP, Proteintech, RRID: AB_2782956), myelocytomatosis oncogene (c-MYC; 10828-1-AP, Proteintech, RRID: AB_2148585), protein kinase B/AKT (PKB/AKT; #9272, Cell Signaling Technology, RRID: AB_329827), phospho-AKT (Ser473) (p(S473) AKT; #9271, Cell Signaling Technology, RRID: AB_329825), phospho-AKT (Thr308) (p(T308) AKT; #9275, Cell Signaling Technology, RRID: AB_329828), Glyceraldehyde-3-phosphate dehydrogenase (GAPDH; #5174, Cell Signaling Technology, RRID: AB_10622025), Na^+/K^+ ATPase (#3010, Cell Signaling Technology, RRID: AB_2060983), TATA-binding protein (TBP; 22006-1-AP, Proteintech, RRID: AB_10951514), and β-ACTIN (sc-1616; Santa Cruz Biotechnology, RRID: AB_630836). Specific antigen-antibody complexes were visualized using horseradish-peroxidase-conjugated anti-rabbit antibodies (ab97051, Abcam, RRID: AB_2202239) against CBS, CTH, xCT, DNMT1, DNMT3A, DNMT3B, ATF4, NRF2, GAPDH, Na^+/K^+ ATPase, and TBP or anti-mouse antibodies (sc-2005, Santa Cruz Biotechnology, RRID: AB_631736) against GCLC, GCLM, and ImmunoStar LD (Fujifilm Wako Pure Chemical). The membranes were photographed, and the density of each band was analyzed using ImageQuant LAS4010 (GE Healthcare Life Sciences, Buckinghamshire, UK) and ImageJ software.

Quantitative RT-PCR analysis

Total RNA was extracted from cultured cells using RNA iso Plus (Takara Bio Inc, Shiga, Japan) according to the manufacturer's instructions. We also commercially obtained RNA samples derived human healthy liver (Fujifilm Wako Pure Chemical). Complementary DNA (cDNA) was synthesized by reverse transcription using the ReverTra Ace qPCR RT kit (Toyobo, Osaka, Japan). Real-time PCR analysis was performed on diluted cDNA samples using THUNDERBIRD SYBR qPCR Mix (Toyobo) and the LightCycler 96 system (Roche Diagnostics, Basel, Schweiz). Data were normalized using *18s* rRNA, and the primer sequences are listed in Supplementary Table S2.

Measurement of the intracellular ROS levels

Hepatocytes were isolated from male BALB/c mice using the collagenase perfusion method and plated in 96-well black plates. The medium was changed after 4 h of incubation. The next day, hepatocytes were treated with PAG for 0, 6, 12, 18, and 24 h. Intracellular reactive oxygen species (ROS) levels in primary hepatocytes were evaluated at the same time using the ROS Assay Kit, Highly Sensitive DCFH-DA (Dojindo), following the manufacturer's instructions. The fluorescence activity of DCFH-DA was measured using an EnSpire Multimode Plate Reader and was normalized to Hoechst33342 (Dojindo).

Statistical analysis

All statistical analyses were performed using JMP pro17.0 (SAS Institute Japan, Tokyo, Japan). The significance of

differences among groups was analyzed using one-way or two-way ANOVA, followed by Tukey–Kramer's post hoc test. Student's *t*-test was used to compare data between the two groups. A 5% level of probability was considered to be statistically significant.

Results

Oncogenic alterations in the expression of *CBS*, *CTH*, and *SLC7A11* in cancer patients

Intracellular cysteine levels are mainly dependent on intracellular synthesis from methionine through the trans-sulfuration pathway and the exogenous supply of cystine uptake provided by the cystine/glutamate antiporter xCT (Fig. 1A) [6]. Analysis of RNA-seq data from patients with hepatocarcinoma using the TNMplot database revealed that the expressions of de novo cysteine synthetases, *CBS* and *CTH*, were down-regulated in hepatic tumor cells. Conversely, the expression of *SLC7A11*, encoding xCT, was up-regulated in the hepatic tumors (Fig. 1B). Similar alterations of gene expressions were observed in breast carcinoma, renal carcinoma, pancreatic adenocarcinoma, and stomach adenocarcinoma (Supplementary Fig. S1). The degree of decreased expression for *CBS* and *CTH*, and the degree of increased expression for *SLC7A11*, were more pronounced with the malignancy of hepatocarcinoma (Fig. 1C). Furthermore, the alterations of these gene expressions were associated with a poor prognosis for patients with hepatocarcinoma (Fig. 1D). Consistent with these results, we also detected the down-regulation of *CBS* and *CTH* and the up-regulation of *SLC7A11* in the human hepatocarcinoma cell line, HepG2 and HepaRG (Fig. 1E). These results reveal the implication of oncogenic alterations of cysteine metabolism in the malignancy of hepatocarcinoma, as well as in other types of cancer.

BNL 1ME A.7 R.1-bearing mice show similar alterations of cysteine metabolism in patients with hepatocarcinoma

To investigate the underlying mechanism of the oncogenic alteration of cysteine metabolism, we prepared a syngeneic mouse model of hepatocarcinoma. BNL 1ME A.7 R.1 cells are a murine hepatocarcinoma cell line generated by the treatment of BALB/c mice-derived hepatocytes with the chemical carcinogen, methylcholanthrene epoxide [15, 16]. We implanted the hepatocarcinoma cells into the back of male BALB/c mice. After tumor formation, we assessed the protein expression levels of cysteine synthetic enzymes, xCT, and glutathione synthetic enzymes in the liver and BNL 1ME A.7 R.1-formed tumors in mice. As observed in patients with hepatocarcinoma, the protein levels of CBS and CTH were down-regulated in BNL 1ME A.7 R.1-formed tumors, and the protein levels of xCT were up-regulated in hepatic tumor cells (Fig. 2A). In addition, the cysteine and cystine levels were increased in hepatic tumor cells, whereas the intratumoral glutathione levels were significantly decreased (Fig. 2B). The decreased glutathione levels may be due to the down-regulation of the protein levels for the rate-limiting enzymes of glutathione synthesis, GCLC and GCLM (Fig. 2A). These results suggest that oncogenic transformation of hepatocytes induces a shift in intracellular cysteine supply pathway from the de novo synthesis to extracellular uptake. This metabolic reprogramming appeared to result in intra-tumoral cysteine accumulation. Therefore, we used this hepatocarcinoma animal model to investigate the mechanism underlying oncogenic alterations in cysteine metabolism.

Epigenetic repression of genes involved in de novo cysteine synthesis in hepatocarcinoma cells

The expressions of CBS and CTH are regulated through transcriptional and translational processes [23]. DNA methylation of the promoter regions of *CBS* and *CTH* genes is thought to repress their expressions in stomach or liver cancer in humans [24, 25]. Significant reductions in the *Cbs* and *Cth* mRNA levels were also observed in BNL 1ME A.7 R.1-formed tumors in mice (Fig. 3A). Therefore, we investigated the DNA methylation status of the upstream regions in the mouse *Cbs* and *Cth* genes of BNL 1ME A.7 R.1 cells. DNA methylation is mainly catalyzed by three enzymes; DNMT1, DNMT3A, and DNMT3B [26]. DNMT3A and DNMT3B catalyze de novo DNA methylation, whereas DNMT1 maintains the DNA methylation status during cell proliferation. The mRNA expression levels of these three DNA methyltransferases were up-regulated in BNL 1ME A.7 R.1-formed tumors (Fig. 3B). In addition, significant increase in the methionine and *S*-adenosylmethionine levels were also detected in BNL 1ME A.7 R.1-formed tumors (Supplementary Fig. S2). Because several CpG islands are located in the upstream regions of the mouse *Cbs* and *Cth* genes, we investigated their DNA methylation statuses by direct-bisulfite sequencing [27, 28]. The methylation levels for the upstream region of the mouse *Cbs* gene spanning from −171 to −84 bp (relative to the transcription start site, +1) and mouse *Cth* gene spanning from −335 to −265 bp were increased in BNL 1ME A.7 R.1-formed tumors (Fig. 3C and D).

Treatment of cultured BNL 1ME A.7 R.1 cells with a DNA methyltransferase inhibitor, decitabine, decreased methylation levels for the upstream regions of *Cbs* and *Cth* genes (Supplementary Fig. S3A) and restored their expression levels (Fig. 4A and B), although the restoration levels of CBS and CTH were insufficient with for increasing intracellular cysteine levels (Supplementary Fig. S3B). Furthermore, the down-regulation of DNA methyltransferases by shRNA restored the expression levels for *Cbs* and *Cth* mRNAs (Fig. 4C) and their

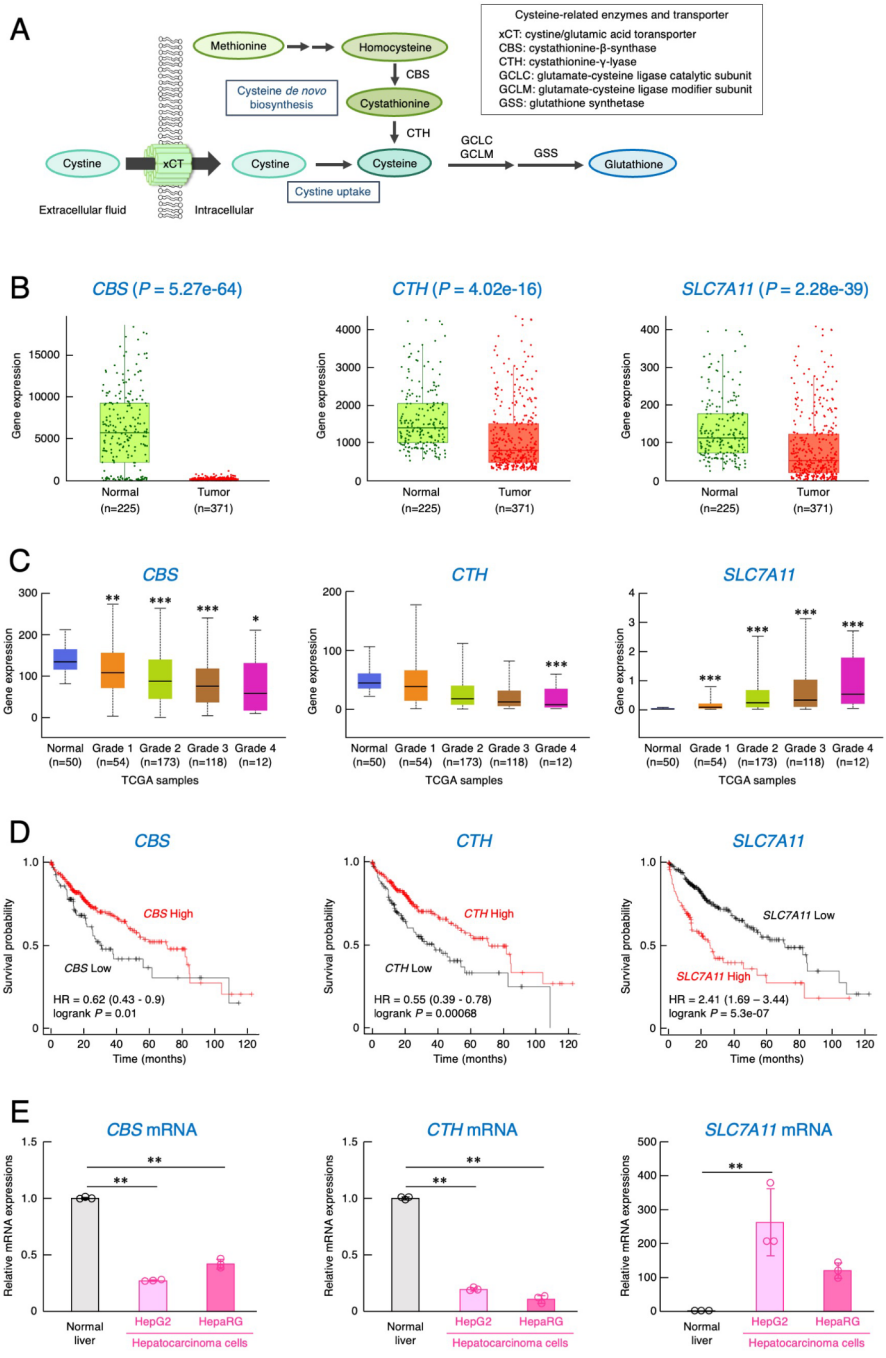

Fig. 1 Oncogenic alterations in the expression of *CBS*, *CTH*, and *SLC7A11* genes in patients with hepatocarcinoma. **A**, Schematic illustrating the cysteine metabolic pathways. Cysteine is synthesized from methionine or converted from cystine that is uptaken by xCT from the extracellular fluid. Cysteine is also used for glutathione synthesis. **B**, Differences in the expression of *CBS*, *CTH*, and *SLC7A11* genes in the liver and hepatic tumors. RNA-seq data obtained from patients with hepatocarcinoma were analyzed using the TNMplot database. *P*-values were calculated using the Mann–Whitney U-test. **C**, Tumor grade-dependent expression of *CBS*, *CTH*, and *SLC7A11* genes in liver hepatocellular carcinoma (LIHC) patients. TCGA samples were analyzed using the UALCAN database. Grade 1, well-differentiated (low grade); grade 2, moderately differentiated (intermediate grade); grade 3, poorly differentiated (high grade); grade 4, undifferentiated (high grade). ***$P < 0.001$, **$P < 0.01$, *$P < 0.05$; significant difference compared with the normal group (unpaired *t*-test). **D**, Prognostic significance of the expression for *CBS*, *CTH*, and *SLC7A11* genes in LIHC patients analyzed using the Kaplan–Meier plotter database. Hazard ratios with 95% confidence intervals and log-rank *P*-values were calculated using Kaplan–Meier plots. **E**, The mRNA levels of genes involved in cysteine metabolism in the human normal hepatocytes, HepG2 cells, and HepaRG cells. The expression levels were normalized to those of *18s*. The values in the human normal liver were set at 1.0. Each value represents the mean with S.D. ($n = 3$). **$P < 0.01$; significant difference between the indicated groups ($F_{2,6} = 595.045$, $P < 0.001$ for *CBS*; $F_{2,6} = 1572.452$, $P < 0.001$ for *CTH*; $F_{2,6} = 14.902$, $P = 0.005$ for *SLC7A11*; ANOVA with Tukey–Kramer's post hoc test)

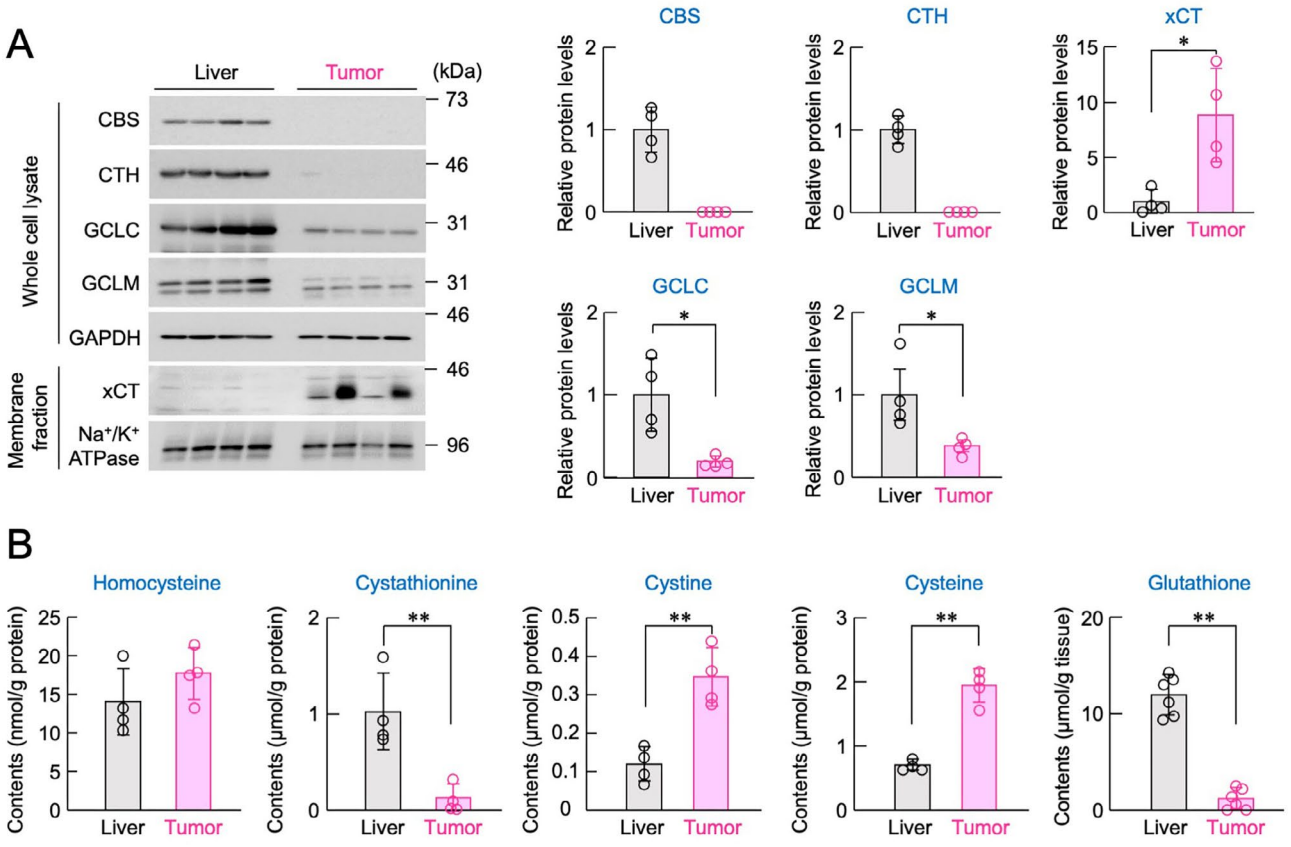

Fig. 2 Oncogenic alterations of cysteine metabolism in murine hepatocarcinoma BNL 1ME A.7 R.1 cells. **A**, The protein levels of genes involved in cysteine metabolism in the liver and BNL 1ME A.7 R.1-formed tumors in mice. The protein levels were normalized to those of GAPDH (for CBS, CTH, GCLC, and GCLM) or Na^+/K^+ ATPase (for xCT). The values in the liver were set at 1.0. Each value represents the mean with S.D. ($n=4$). *$P<0.05$; significant difference between the two groups ($t_6=-3.621$, $P=0.011$ for GCLC; $t_6=-2.788$, $P=0.032$ for GCLM; $t_6=3.594$, $P=0.011$ for xCT; unpaired *t*-test, two sided). **B**, Intracellular contents of cysteine-related metabolites in the liver and BNL 1ME A.7 R.1-formed tumors in mice. Each value represents the mean with S.D. ($n=4$–6). **$P<0.01$; significant difference between the two groups ($t_6=-4.272$, $P=0.005$ for cystathionine; $t_6=5.171$, $P=0.002$ for cystine; $t_6=9.032$, $P=0.001$ for cysteine; $t_{10}=-11.398$, $P<0.001$ for glutathione; unpaired *t*-test, two sided)

proteins in BNL 1ME A.7 R.1 cells (Fig. 4D). Among these, the down-regulation of *Dnmt3a* had significant effects on the expression of both CBS and CTH, whereas *Dnmt1* down-regulation restored only the expression of CBS. These results indicated that DNA methylation contributes to maintaining gene suppression of cysteine synthases in hepatocarcinoma.

Repression of de novo cysteine synthesis up-regulates xCT expression

Despite decreasing de novo synthase activities, cysteine content was increased in BNL 1ME A.7 R.1 cells (Fig. 2B). Consistent with increased xCT expression, cystine uptake activity was enhanced in BNL 1ME A.7 R.1 cells (Fig. 5A). Intracellular cystine is reduced to cysteine and serves as a source for the de novo synthesis of glutathione and proteins [29]. Inhibition of xCT activity by erastin significantly decreased the cysteine content in BNL 1ME A.7 R.1 cells but not in primary cultured hepatocytes (Fig. 5B), suggesting that intra-tumoral accumulation of cysteine depends on the up-regulation of xCT-mediated cystine uptake.

Next, we investigated the mechanism by which xCT expression is up-regulated in hepatocellular carcinoma cells with repressed de novo cysteine synthesis. Treatment of primary cultured hepatocytes prepared from the liver of BALB/c mice with the CBS inhibitor aminooxy acetic acid (AOAA) or the CTH inhibitor propargylglycine (PAG) decreased intracellular cysteine levels, revealing the suppression of de novo cysteine synthesis (Supplementary Fig. S4A and S4B). Treatment with PAG, but not with AOAA, significantly increased the expression levels of *Slc7a11* mRNA (Fig. 5C) and xCT protein (Fig. 5D). These findings suggested that repression of de novo cysteine synthesis repulsively increases xCT expression.

Since repression of de novo cysteine synthesis by PAG increased xCT expression at the mRNA level, we focused on the transcriptional activity of the *Slc7a11* gene. Activating transcription factor-4 (ATF4) or NF-E2-related

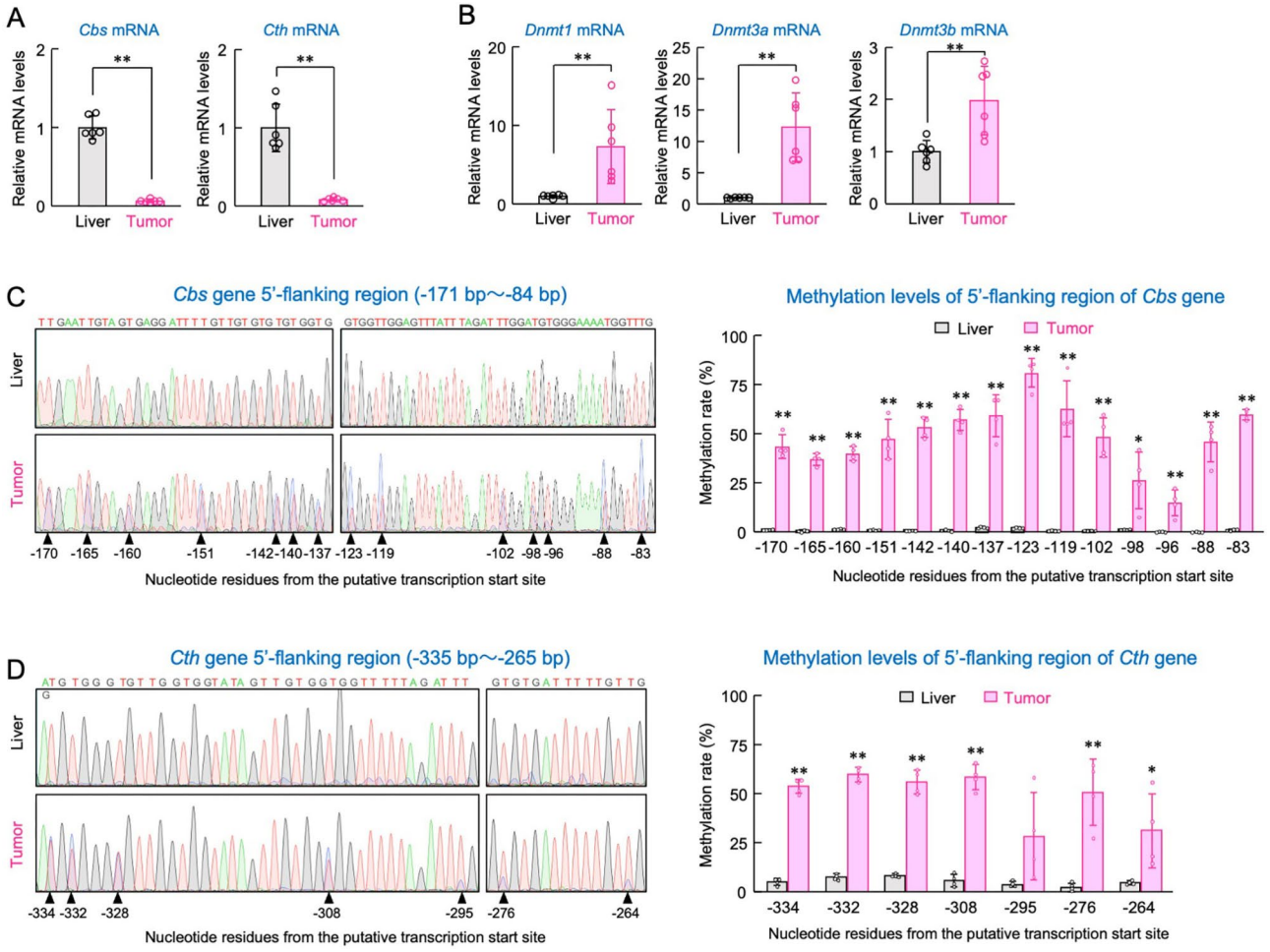

Fig. 3 Epigenetic modifications of the 5′-flanking region of the cysteine synthetic genes in the hepatic tumors. **A** and **B**, The mRNA levels of the enzymes involved in cysteine synthesis (**A**) and DNA methyltransferases (**B**) in the liver and BNL 1ME A.7 R.1-formed tumors in mice. The expression levels were normalized to those of *18s*. The values in the liver were set at 1.0. Each value represents the mean with S.D. ($n=6$). $^{**}P<0.01$; significant difference between the two groups ($t_{10}=-15.397$, $P<0.001$ for *Cbs*; $t_{10}=-7.424$, $P<0.001$ for *Cth*; $t_{10}=-3.258$, $P=0.009$ for *Dnmt1*; $t_{10}=5.041$, $P=0.001$ for *Dnmt3a*; $t_{10}=-3.438$, $P=0.006$ for *Dnmt3b*; unpaired *t*-test, two sided). **C** and **D**, Methylation status of the 5′-flanking region in mice *Cbs* (C) and *Cth* (D) genes in the BNL 1ME A.7 R.1-formed tumors. Left panels show representative electropherograms of direct-bisulfite sequencing. Triangles indicate the methylation sites. Right panels show the quantification of methylation levels. Each value represents the mean with S.D. ($n=4$). $^{**}P<0.01$, $^{*}P<0.05$; significant difference between the two groups (unpaired *t*-test, two sided)

factor 2 (NRF2) induces xCT expression [11, 30]. ATF4 is a main downstream effector of general control nonderepressible 2 (GCN2), a sensor of amino acid deprivation, and regulates the expression and activity of genes involved in amino acid transport [11]. NRF2 is also activated in response to oxidative stress, hypoxia, and cell growth signaling [30] and induces the expression of cytoprotective enzymes and transporters involving xCT [31]. Although ATF4 was undetectable in BNL 1ME A.7 R.1-formed tumors in mice, the expression of NRF2 markedly increased in the tumors (Fig. 5E). Down-regulation of NRF2 by siRNA significantly decreased the expression of xCT in BNL 1ME A.7 R.1 cells (Fig. 5F), suggesting that NRF2 acts as a transcriptional activator of xCT in oncogenic transformed hepatocytes.

Inhibition of extracellular cystine supply suppresses the growth of BNL 1ME A.7 R.1-formed tumors in mice

In the final set of experiments, we investigated how inhibition of the extracellular cysteine supply affects the growth of hepatocarcinoma-formed tumors. Down-regulation of xCT by shRNA partially suppressed the growth of cultured BNL 1ME A.7 R.1 cells (Fig. 6A). The treatment with 1.5 μM erastin also repressed their growth and decreased intracellular cysteine levels, but had a negligible effect on the cell viability and cysteine content of primary culture hepatocytes (Figs. 5B and 6B and C). Therefore, we explored whether inhibition of the extracellular cysteine supply prevents the growth of hepatocarcinoma-formed tumors in mice. To achieve this, we administrated erastin (30 mg/kg body weight, i.p) to BNL 1ME A.7 R.1-inoculated BALB/c mice every three

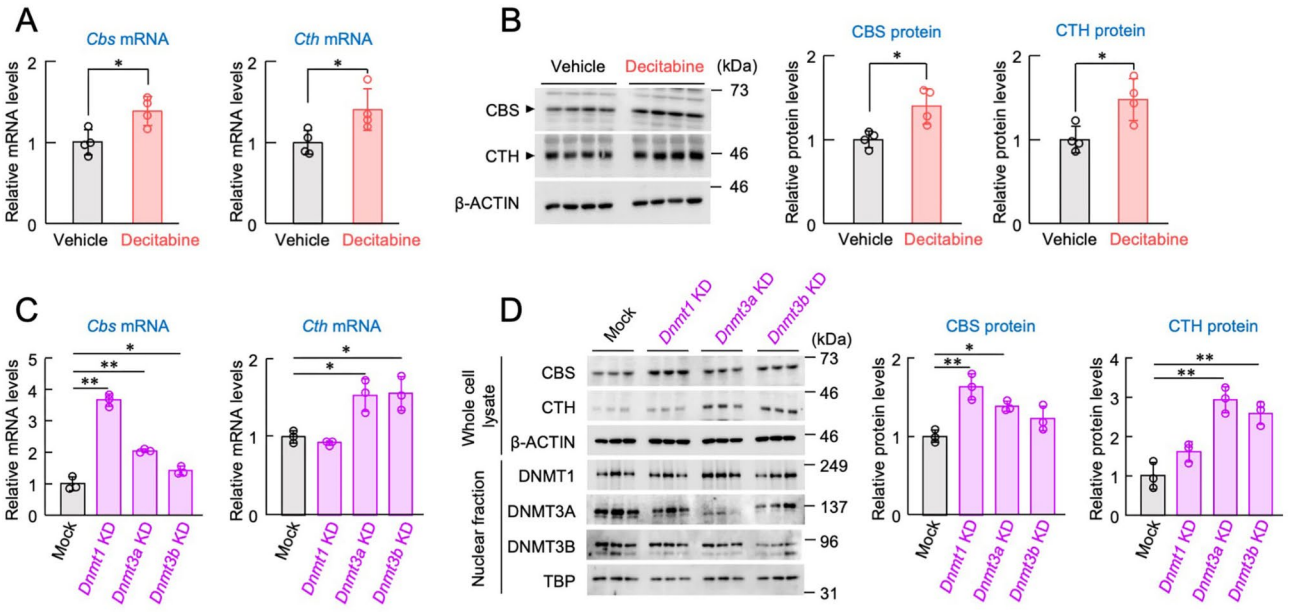

Fig. 4 DNA methyltransferase suppresses the expression of cysteine synthetic enzymes in BNL 1ME A.7 R.1 cells. **A** and **B**, Induction of CBS and CTH expression by pharmacological inhibition of DNA methyltransferase activity. BNL 1ME A.7 R.1 cells were treated with 500 nM decitabine for 24 h. The mRNA and protein levels were normalized to those of *18s* and β-ACTIN, respectively. The values in vehicle-treated cells were set at 1.0. Each value represents the mean with S.D. ($n=4$). *$P<0.05$; significant difference between the two groups ($t_6=2.719$, $P=0.035$ for *Cth* mRNA; $t_6=3.498$, $P=0.013$ for CBS protein; $t_6=3.270$, $P=0.017$ for CTH protein; unpaired *t*-test, two sided). **C** and **D**, Induction of CBS and CTH expressions by down-regulation of DNA methyltransferase. BNL 1ME A.7 R.1 cells were transduced with lentivirus expressing shRNA against *Dnmt1*, *Dnmt3a*, or *Dnmt3b*. The mRNA and protein levels in mock-transduced and *Dnmt*-knockdown (KD) cells were normalized to those of *18s* and β-ACTIN, respectively. The values in mock-transduced cells were set at 1.0. Each value represents the mean with S.D. ($n=3$). **$P<0.01$, *$P<0.05$; significant difference between the indicated groups ($F_{3,8}=160.673$, $P<0.001$ for *Cbs* mRNA; $F_{3,8}=13.969$, $P=0.002$ for *Cth* mRNA; $F_{3,8}=13.491$, $P=0.002$ for CBS protein; $F_{3,8}=24.930$, $P<0.001$ for CTH protein; ANOVA with Tukey–Kramer's post hoc test)

days, which suppressed the growth of BNL 1ME A.7 R.1-formed tumors (Fig. 6D). The tumor volume on day 15 after the initiation of erastin administration was significantly smaller than that observed in mice treated with vehicle, suggesting that the growth of oncogenic transformed hepatic cells depends on the extracellular cysteine supply. Oncogenic alteration of the cysteine supply pathway from intracellular de novo synthesis to extracellular uptake may be necessary for cancer cells to rapidly proliferate and resist oxidative stress.

Discussion

Owing to their abnormal growth and rapid proliferation, cancer cells are exposed to an environment distinct from that of normal healthy cells, characterized by hypoxia, acidity, and low nutrient levels [32]. To adapt to such an environment, cancer cells undergo metabolic reprogramming [33], and alterations in cysteine metabolism are often observed in oncogenic transformed cells [34]. In the present study, we observed decreased expression of genes involved in de novo cysteine synthesis and increased expression of the cystine uptake transporter xCT by analyzing a database of patients with hepatocarcinoma, breast invasive carcinoma, kidney renal clear cell carcinoma, pancreatic adenocarcinoma, and gastric adenocarcinoma. Consistent with these findings, BNL 1ME A.7 R.1-bearing mice exhibited similar alterations in the expression of genes involved in cysteine metabolism. Employing this animal model of hepatocarcinoma, we demonstrated that epigenetic repression of de novo cysteine synthases up-regulates the expression of the extracellular cystine uptake transporter xCT and subsequent intracellular cysteine accumulation (Fig. 7).

In healthy cells, cysteine is synthesized from methionine through the trans-sulfuration pathway. CBS and CTH play critical roles in catalyzing the transformations of homocysteine to cystathionine and cystathionine to cysteine, respectively [35]. The expressions of CBS and CTH were down-regulated in hepatocarcinoma-formed tumors in both humans and animal models. A previous study has demonstrated that DNA methylation status is negatively correlated with CBS expression levels in cancer cells [24]. Although reduced expression of genes involved in de novo cysteine synthesis has been detected in various types of cancers, this phenomenon appears to depend on differences in the origin of cancer [12]. The methylation status of genomic DNA is also subject to variation, not only because of congenital factors but also as a result of acquired influences [36]. DNA methyltransferases (DNMTs) are a conserved family of cytosine

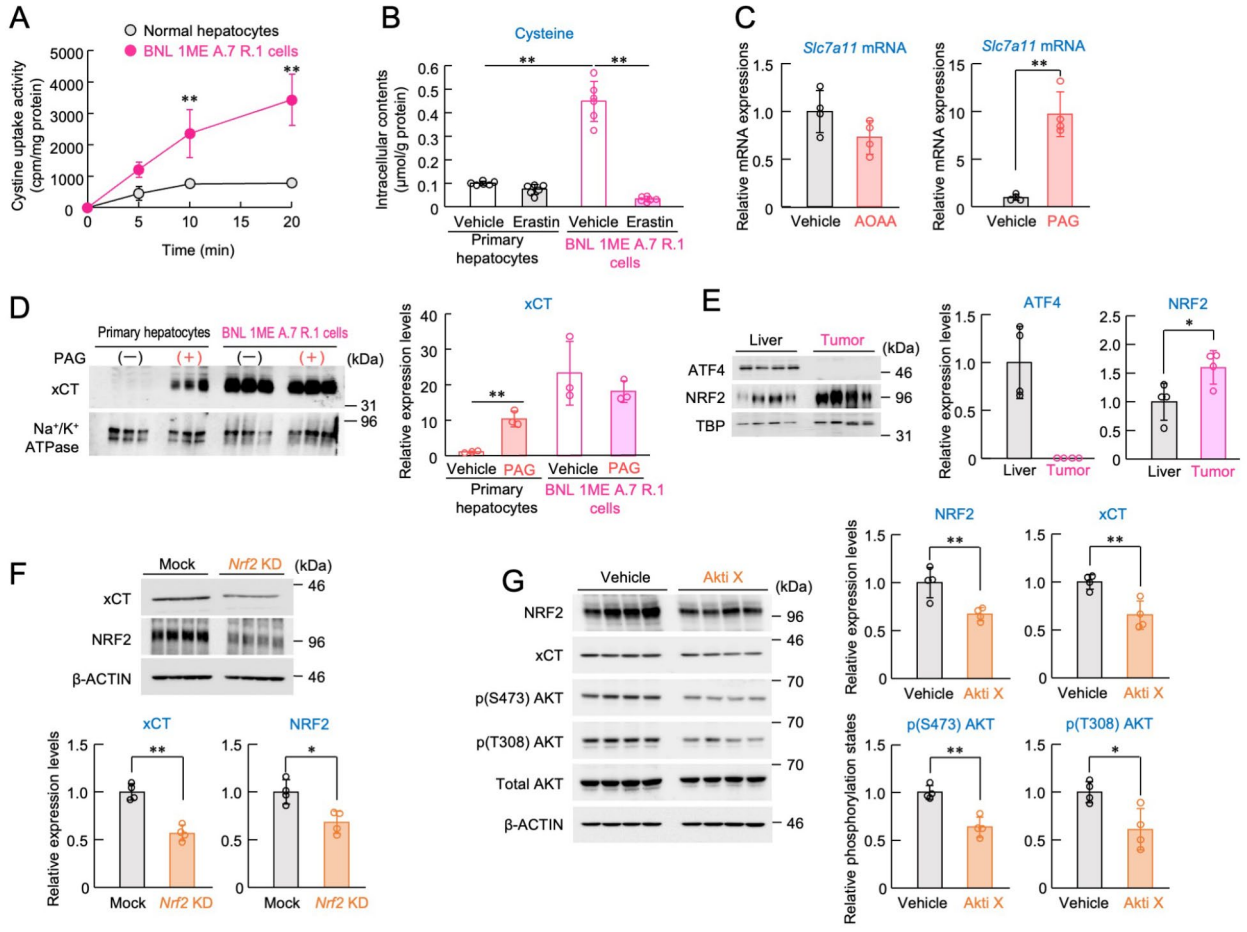

Fig. 5 Reduction of cysteine synthase activity induces xCT expression by up-regulating NRF2. **A**, The transporting activity of xCT in normal hepatocytes and BNL 1ME A.7 R.1 cells prepared from tumor-bearing mice. Each value represents the mean with S.D. ($n=4$). $^{**}P<0.01$; significant difference compared with the normal hepatocytes at the corresponding times ($F_{2,18}=7.921$; $P<0.001$; Two-way ANOVA with Tukey–Kramer's post hoc test). **B**, Intracellular cysteine contents in primary hepatocytes and BNL 1ME A.7 R.1 cells after treatment with 1.5 μM erastin. Each value represents the mean with S.D. ($n=6$). $^{**}P<0.01$; significant difference between the two groups ($F_{3,20}=112.712$, $P<0.001$; ANOVA with Tukey–Kramer's post hoc test). **C**, The mRNA levels of *Slc7a11* in primary hepatocytes after treatment with 1.5 mM AOAA or 1.0 mM PAG for 24 h. Each value represents the mean with S.D. ($n=4$). $^{**}P<0.01$; significant difference between the two groups ($t_6=7.297$, $P<0.001$; unpaired *t*-test, two sided). **D**, The protein levels of xCT in primary hepatocytes and BNL 1ME A.7 R.1 cells after treatment with 1.0 mM PAG for 24 h. Each value represents the mean with S.D. ($n=4$). $^{**}P<0.01$; significant difference between the two groups ($t_4=7.301$, $P=0.002$; unpaired *t*-test, two sided). **E**, The protein levels of ATF4 and NRF2 in the liver and hepatic tumors. Each value represents the mean with S.D. ($n=4$). $^{*}P<0.05$; significant difference between the two groups ($t_6=2.748$, $P=0.033$; unpaired *t*-test, two sided). **F**, The protein levels of xCT and NRF2 in mock-transfected or *Nrf2*-knockdown (KD) BNL 1ME A.7 R.1 cells. Each value represents the mean with S.D. ($n=4$). $^{**}P<0.01$, $^{*}P<0.05$; significant difference between the two groups ($t_6=-7.171$, $P<0.001$ for xCT; $t_6=-3.664$, $P=0.011$ for NRF2; unpaired *t*-test, two sided). **G**, The protein levels of NRF2, xCT and phosphorylation states of AKT protein in BNL 1ME A.7 R.1 cells after treatment with 10 μM Akti X for 48 h. The protein levels were normalized to those of β-ACTIN (for NRF2 and xCT) or total AKT (for p(S473) AKT and p(T308) AKT). The values in vehicle-treated cells were set at 1.0. Each value represents the mean with S.D. ($n=4$). $^{**}P<0.01$, $^{*}P<0.05$; significant difference between the two groups ($t_6=-5.694$, $P=0.013$ for p(S473) AKT; $t_6=-3.227$, $P=0.018$ for p(T308) AKT; $t_6=-3.874$, $P=0.008$ for NRF2; $t_6=-4.126$, $P=0.006$ for xCT; unpaired *t*-test, two sided)

methylases with a key role in the epigenetic regulation of gene expression [26]. Elevated levels of DNMTs appeared to repress the expression of CBS and CTH in hepatocarcinoma tumors in mice. *Dnmt3a* downregulation had a significant effect on the expression of both CBS and CTH, whereas *Dnmt1* downregulation only restored the expression of CBS. These observations indicated the differential contribution of each DNMT subtype to the expression of CBS and CTH. Several oncogenic transcription factors, including SP1, FOXC1, and c-MYC, have been reported to up-regulate the expression of DNMTs in cancer cells [37]. Compared to normal healthy hepatocytes, we observed increased expression of c-MYC in BNL 1ME A.7 R.1 cells (Supplementary Fig. S5). This may account for the up-regulation of DNMTs and the increased methylation status of *Cbs* and *Cth* genes. However, the expressions of these cysteine synthesis enzymes were not fully restored by the down-regulation

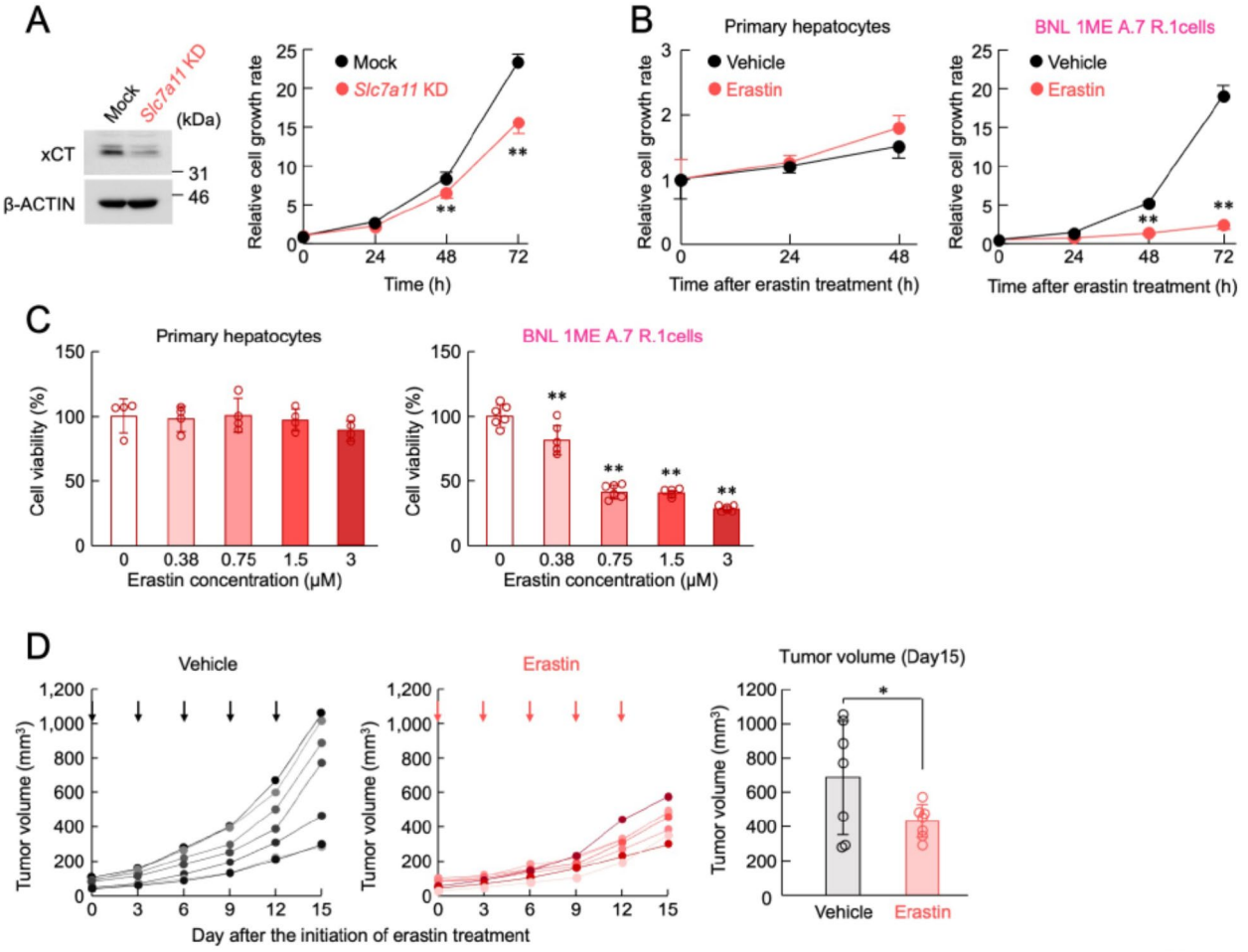

Fig. 6 Pharmacological inhibition of extracellular cystine supply represses the growth of hepatocarcinoma cells. **A**, The proliferation of mock-transduced or *Slc7a11*-knockdown (KD) BNL 1ME A.7 R.1 cells. The basal cell viability (0 h) of mock-transduced cells was set at 1.0. Each value represents the mean with S.D. ($n = 6$). $^{**}P < 0.01$; significant difference between the two groups ($F_{3,40} = 69.532$; $P < 0.0001$; Two-way ANOVA with Tukey–Kramer's post hoc test). **B**, The proliferation of primary hepatocytes and BNL 1ME A.7 R.1 cells during incubation in media in the presence or absence of 1.5 μM erastin. The basal cell viability (0 h) of vehicle-treated cells was set at 1.0. Each value represents the mean with S.D. ($n = 6$). $^{**}P < 0.01$; significant difference between the two groups ($F_{2,30} = 104.061$, $^{**}P < 0.001$; Two-way ANOVA with Tukey–Kramer's post hoc test). **C**, The cell viability of primary hepatocyte and BNL 1ME A.7 R.1 cells after incubation in medium containing the indicated concentrations of erastin for 24 h. The viability of cells incubated in the absence of erastin (0 μM) was set at 100%. Each value represents the mean with S.D. ($n = 4$–6). $^{**}P < 0.01$; significant difference from the group of cells incubated in the absence of erastin (Dunnett's test). **D**, The growth of BNL 1ME A.7 R.1-formed tumors implanted in mice during the repetitive administration of erastin (30 mg/kg body weight) or vehicle (10% dimethyl sulfoxide, 50% polyethylene glycol in saline). Left and middle panels show individual tumor volumes during administration of erastin or vehicle. The arrows indicate drug administration. Right panel shows the tumor volume 15 days after the initiation of erastin administration. Each value represents the mean with S.D. ($n = 7$). $^{*}P < 0.05$; significant difference between the two groups ($F_{11,72} = 15.816$, $P < 0.001$; One-way ANOVA with Tukey–Kramer's post hoc test)

of DNMTs in BNL 1ME A.7 R.1 cells. Therefore, other factors may also directly or indirectly suppress the de novo cysteine synthetase activities in BNL 1ME A.7 R.1 cells. Further studies are required to investigate the exact mechanism underlying the decreased expressions of CBS and CTH in transformed oncogenic cells.

Because the decreased expression of de novo cysteine synthases was accompanied by up-regulation of the cystine uptake transporter xCT, we investigated the possibility that repression of de novo cysteine synthesis plays a role in maintaining or increasing its intracellular concentration by enhancing cystine uptake from the extracellular environment. Inhibition of de novo cysteine synthesis by the treatment of primary hepatocytes with CTH inhibitor PAG increased the expression of *Slc7a11* mRNA and xCT protein, accompanied by elevated NRF2 levels. Cancer cells constitutively activate NRF2 through various mechanisms, including somatic mutations, epigenetic silencing degradation, and transcriptional activation by oncogene-mediated signaling [38]. Under normal healthy conditions, NRF2 binds to KEAP1, leading to constitutive ubiquitination and proteasomal degradation.

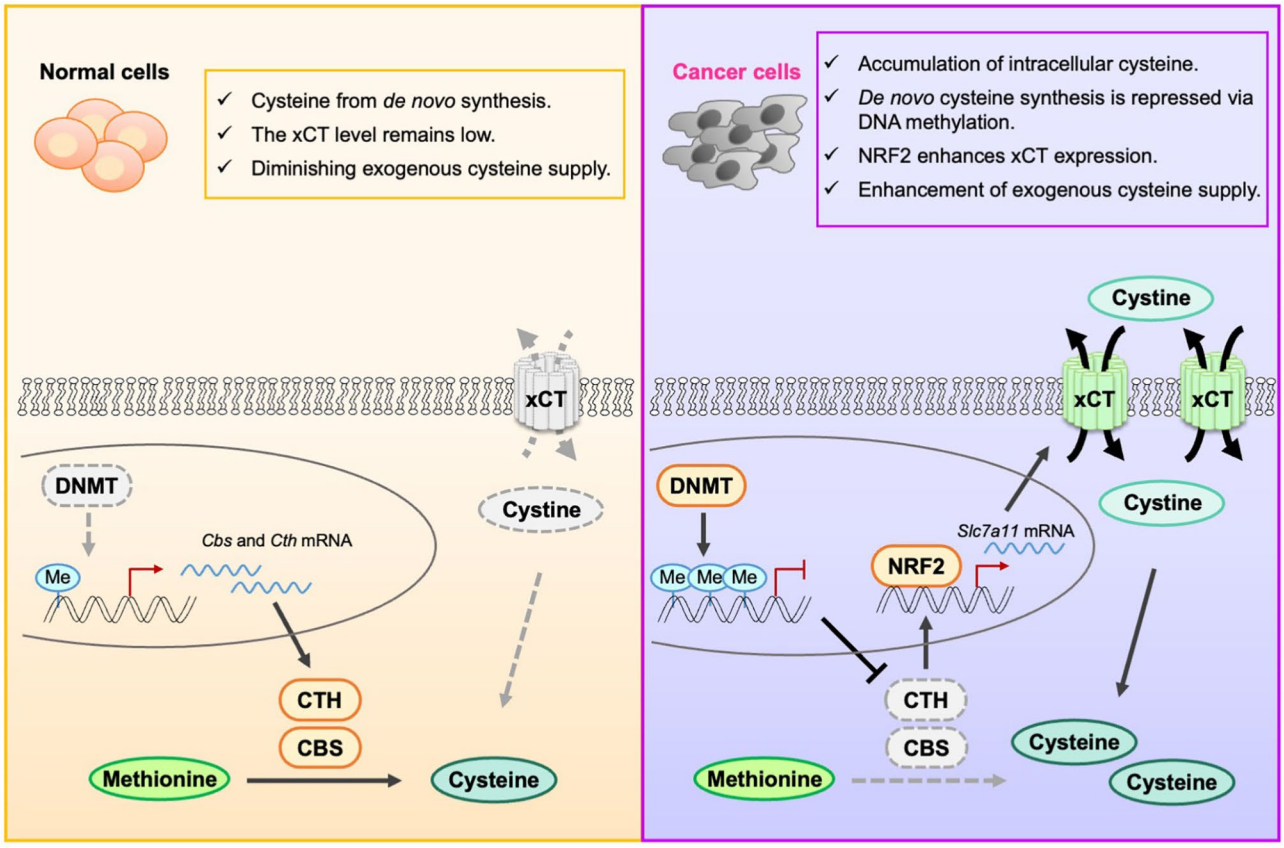

Fig. 7 Schematic diagram of oncogenic alteration of cysteine metabolism in hepatocarcinoma. de novo cysteine synthesis in BNL 1ME A.7 R.1 cells is repressed by DNA hypermethylation of the *Cbs* and *Cth* genes. Decreased de novo synthase activities increase cystine uptake by up-regulating NRF2-mediated xCT expression. This metabolic cysteine reprogramming may be required for the rapid proliferation and survival of cancer cells of oncogenic transformed cells

Reactive oxygen species (ROS) are well known molecules that increase the intracellular NRF2 levels [39]. ROS can oxidize the cysteine residues in KEAP1, inducing a conformational change in KEAP1 and releasing NRF2 [40]. Furthermore, deprivation of intracellular cysteine results in ROS accumulation [41], which stabilizes NRF2 by preventing its degradation. Activated NRF2 translocates into the nucleus and induces the expression of its target gene, involving *Slc7a11*. However, no significant accumulation of ROS was observed in primary hepatocytes when cells were treated with CTH inhibitor PAG (Supplementary Fig. S6A). On the other hand, glycogen synthase kinase-3β (GSK3β) also participates in NRF2 degradation [42], and the GSK3β-mediated degradation of NRF2 is prevented by protein kinase B (PKB)/AKT signaling [43]. Previous studies have demonstrated that the inhibition of CTH activity stimulates PKB/AKT signaling [44]. Herein, the phosphorylation state of PKB/AKT was enhanced in BNL 1ME A.7 R.1 cells (Supplementary Fig. S6B), indicating activation of the protein kinase in hepatocarcinoma, and treatment with PKB/AKT inhibitor Akti X diminished NRF2 accumulation and decreased xCT expression levels (Fig. 5G). Although it remains to be clarified how CTH inhibition can activate PKB/AKT signaling, up-regulation of this protein kinase contributes to the elevation of NRF2 levels and expression of xCT in BNL 1ME A.7 R.1 cells. Importantly, elevation of NRF2 levels were unlikely to feedback on the expressions of de novo cysteine synthases because treatment of primary hepatocytes with NRF2 degradation inhibitor, 4-octyl itaconate, had a negligible effect on the expression of CBS and CTH proteins as well as cell viability (Supplementary Fig. S7).

Cysteine plays various roles in the maintenance of cellular functions, but it is also known to enable glutathione biosynthesis. Cancer cells intrinsically exhibit enhanced ROS production for various reasons, including genetic aberrations, rapid proliferation, and altered cellular metabolism [45]. Enhanced production of ROS promotes tumor growth and progression [46]; however, above the cytotoxic threshold, ROS-induced oxidative stresses result in apoptotic death or senescence of cancer cells. Therefore, cancer cells can maintain ROS levels below a cytotoxic threshold by enhancing the biosynthesis of

antioxidants such as glutathione [47]. The present study indicated that oncogenic transformation of hepatocytes induces a shift in the intracellular cysteine supply pathway from de novo synthesis to extracellular uptake. Indeed, the intracellular cysteine levels of cultured BNL 1ME A.7 R.1 cells and their proliferation were increased in an extracellular cystine concentration-dependent manner (Supplementary Fig. S8). Metabolic reprogramming appears to result in intra-tumoral cysteine accumulation. As the capacity for intracellular cysteine synthesis is limited, the enhancement of extracellular cystine uptake may promote excess antioxidant production in cancer cells. However, the glutathione contents in BNL 1ME A.7 R.1-formed tumors were significantly lower than those in a normal healthy liver, suggesting that cancer cells increase intracellular cysteine levels for purposes other than glutathione synthesis. Cysteine can eliminate intracellular ROS, either by itself or through the production of coenzyme A [48, 49]. In addition, cysteine can induce the expression of insulin growth factor 1 (IGF-1), which acts as a stimulating signal for the proliferation of cancer cells [50]. Deprivation of cystine from the culture media decreased intracellular contents of coenzyme A and the expression levels of *Igf-1* in BNL 1ME A.7 R.1 cells (Supplementary Fig. S9). Therefore, cancer cells, particularly those characterized by intracellular cysteine accumulation and decreased glutathione levels, may use cysteine to synthesize other bioactive molecules that contribute to their survival and proliferation. This notion is also supported by the present findings, which show that inhibition of extracellular cystine uptake by erastin significantly suppresses the growth of BNL 1ME A.7 R.1-formed tumors. Although the inhibition of extracellular cystine uptake is known to induce ferroptotic cell death [51], the differential dependence on extracellular cystine uptake between cancer and normal cells suggests the potential utility of this pathway as a therapeutic target.

Pharmacological inhibition of xCT activity prevents the growth of cultured cancer cells and tumor-implanted animal models [52]. The present results reveal a mechanism for oncogenic alteration of cysteine metabolism and further support the use of xCT as a therapeutic target for the treatment of malignant cancers.

Conclusions

Epigenetic repression of gene responsible for de novo cysteine synthesis repulsively increases cystine uptake via increased xCT expression in hepatocarcinoma, leading to intracellular cysteine accumulation, which contributes to rapid cancer cell proliferation and resistance to oxidative stress. The pharmacological inhibition of xCT activity effectively decreased intracellular cysteine levels and suppressed hepatocarcinoma tumor growth in murine models. These findings not only deepen our understanding of the metabolic alterations occurring in hepatocarcinoma but also offer highlight the efficacy of alteration of cysteine metabolism as a viable therapeutic target in cancer.

Supplementary Information

The online version contains supplementary material available at https://doi.org/10.1186/s40170-024-00352-4.

Supplementary Material 1

Acknowledgements

We are grateful for the technical support provided by the Research Support Center, Graduate School of Medical Sciences, Kyushu University. We thank Soma Yamauchi for technical assistance with the LC-MS/MS analysis.

Author contributions

T. Yamauchi: conceptualization, resources, data curation, formal analysis, supervision, funding acquisition, validation, investigation, visualization, methodology, and writing – original draft. Y. Okano: data curation, formal analysis, investigation, and visualization. D. Terada: data curation, formal analysis, investigation, and visualization. S Yasukochi: data curation, formal analysis, investigation, and visualization. A Tsuruta: methodology. Y Tsurudome: methodology. K Ushijima: methodology. N Matsunaga: methodology. S Koyanagi: supervision, funding acquisition, writing – original draft, project administration, and writing – review and editing. S Ohdo: supervision, funding acquisition, writing– original draft, project administration, and writing – review and editing.

Funding

This study was supported in part by a Grant-in-Aid for Challenging Exploratory Research (22K18375 to S.K.), a Grant-in-Aid for Scientific Research A (22H00442 to S.O.) from the Japan Society for the Promotion of Science, a Grant-in-Aid for Japan Society for the Promotion of Science Fellows (22KJ2383, to T.Y.), and the Platform Project for Supporting Drug Discovery, Life Science Research [Basis for Supporting Innovative Drug Discovery and Life Science Research (BINDS)] from AMED (Grant Number JP24am121031).

Data availability

No datasets were generated or analysed during the current study.

Declarations

Consent for publication

All authors read and approved the final manuscript.

Competing interests

The authors declare no competing interests.

Author details

[1]Department of Pharmaceutics, Faculty of Pharmaceutical Sciences, Kyushu University, Fukuoka, Japan
[2]Department of Clinical Pharmacokinetics, Faculty of Pharmaceutical Sciences, Kyushu University, Fukuoka, Japan
[3]Division of Pharmaceutics, Faculty of Pharmaceutical Sciences, Sanyo-Onoda City University, Yamaguchi, Japan

Received: 21 March 2024 / Accepted: 30 July 2024
Published online: 07 August 2024

References

1. Faubert B, Solmonson A, DeBerardinis RJ. Metabolic reprogramming and cancer progression. Science 2020;368.
2. Yang F, Hilakivi-Clarke L, Shaha A, Wang Y, Wang X, Deng Y, et al. Metabolic reprogramming and its clinical implication for liver cancer. Hepatology. 2023;78:1602–24.

3. Cha YJ, Kim ES, Koo JS. Amino acid transporters and glutamine metabolism in breast cancer. Int J Mol Sci 2018;19.
4. Lieu EL, Nguyen T, Rhyne S, Kim J. Amino acids in cancer. Exp Mol Med. 2020;52:15–30.
5. Butler M, van der Meer LT, van Leeuwen FN. Amino acid depletion therapies: starving cancer cells to death. Trends Endocrinol Metab. 2021;32:367–81.
6. Bonifácio VDB, Pereira SA, Serpa J, Vicente JB. Cysteine metabolic circuitries: druggable targets in cancer. Br J Cancer. 2021;124:862–79.
7. Zhang HF, Klein Geltink RI, Parker SJ, Sorensen PH. Transsulfuration, minor player or crucial for cysteine homeostasis in cancer. Trends Cell Biol 2022;800–14.
8. Combs JA, DeNicola GM. The non-essential amino acid cysteine becomes essential for tumor proliferation and survival. Cancers. 2019;11:678.
9. Chen D, Fan Z, Rauh M, Buchfelder M, Eyupoglu IY, Savaskan N. ATF4 promotes angiogenesis and neuronal cell death and confers ferroptosis in a xCT-dependent manner. Oncogene. 2017;36:5593–608.
10. Zhu H, Blake S, Chan KT, Pearson RB, Kang J. Cystathionine β -Synthase in physiology and Cancer. Biomed Res Int 2018.
11. Koppula P, Zhuang L, Gan B. Cystine transporter SLC7A11/xCT in cancer: ferroptosis, nutrient dependency, and cancer therapy. Protein Cell. 2021;12:599–620.
12. Stipanuk MH, Londono M, Lee JI, Hu M, Yu AF. Enzymes and metabolites of cysteine metabolism in nonhepatic tissues of rats show little response to changes in dietary protein or sulfur amino acid levels. J Nutr. 2002;132:3369–78.
13. Brigham MP, Stein WH, Moore S. The concentrations of cysteine and cystine in human blood plasma. J Clin Invest. 1960;39:1633–8.
14. Yoon SJ, Combs JA, Falzone A, Prieto-Farigua N, Caldwell S, Ackerman HD, et al. Comprehensive metabolic tracing reveals the origin and catabolism of cysteine in mammalian tissues and tumors. Cancer Res. 2023;83:1426–42.
15. Patek PQ, Collins JL, Cohn M. Transformed cell lines susceptible or resistant to in vivo surveillance against tumorigenesis. Nature. 1978;276:510–1.
16. Oh J, Kwak JH, Kwon D, young, Kim AY, Oh DS, Je NK, et al. Transformation of mouse liver cells by methylcholanthrene leads to phenotypic changes associated with epithelial-mesenchymal transition. Toxicol Res. 2014;30:261–6.
17. Bartha Á, Győrffy B. TNMplot.com: a web tool for the comparison of gene expression in normal, tumor and metastatic tissues. Int J Mol Sci. 2021;22:2622.
18. Chandrashekar DS, Karthikeyan SK, Korla PK, Patel H, Shovon AR, Athar M, et al. UALCAN: an update to the integrated cancer data analysis platform. Neoplasia. 2022;25:18–27.
19. Győrffy B. Discovery and ranking of the most robust prognostic biomarkers in serous ovarian cancer. Geroscience. 2023;45:1889–98.
20. Lánczky A, Győrffy B. Web-based survival analysis tool tailored for medical research (KMplot): development and implementation. J Med Internet Res. 2021;23:e27633.
21. Williams GM, Bermudez E, Scaramuzzino D. Rat hepatocyte primary cell cultures. Vitro. 1977;13:809–17.
22. Charni-Natan M, Goldstein I. Protocol for primary mouse hepatocyte isolation. STAR Protoc. 2020;1:100086.
23. Cirino G, Szabo C, Papapetropoulos A. Physiological roles of hydrogen sulfide in mammalian cells, tissues, and organs. Physiol Rev. 2023;103:31–276.
24. Padmanabhan N, Kyon HK, Boot A, Lim K, Srivastava S, Chen S, et al. Highly recurrent CBS epimutations in gastric cancer CpG island methylator phenotypes and inflammation. Genome Biol. 2021;22:167.
25. Lin Z, Huang W, He Q, Li D, Wang Z, Feng Y, et al. FOXC1 promotes HCC proliferation and metastasis by upregulating DNMT3B to induce DNA hypermethylation of CTH promoter. J Exp Clin Can Res. 2021;40:50.
26. Nishiyama A, Nakanishi M. Navigating the DNA methylation landscape of cancer. Trends Genet. 2021;37:1012–27.
27. Smith RWA, Monroe C, Bolnick DA. Detection of cytosine methylation in ancient DNA from five native American populations using bisulfite sequencing. PLoS ONE. 2015;10:e0125344.
28. Weidner L, Lorenz J, Quach S, Braun FK, Rothhammer-Hampl T, Ammer L-M, et al. Translocator protein (18kDA) (TSPO) marks mesenchymal glioblastoma cell populations characterized by elevated numbers of tumor-associated macrophages. Acta Neuropathol Commun. 2023;11:147.
29. Bansal A, Simon MC. Glutathione metabolism in cancer progression and treatment resistance. J Cell Biol. 2018;217:2291–8.
30. Pouremamali F, Pouremamali A, Dadashpour M, Soozangar N, Jeddi F. An update of Nrf2 activators and inhibitors in cancer prevention/promotion. Cell Commun Signal. 2022;20:1–16.
31. Fan Z, Wirth A-K, Chen D, Wruck CJ, Rauh M, Buchfelder M, et al. Nrf2-Keap1 pathway promotes cell proliferation and diminishes ferroptosis. Oncogenesis. 2017;6:e371.
32. Chen Z, Han F, Du Y, Shi H, Zhou W. Hypoxic microenvironment in cancer: molecular mechanisms and therapeutic interventions. Signal Transduct Target Ther. 2023;8:70.
33. Pavlova NN, Zhu J, Thompson CB. The hallmarks of cancer metabolism: still emerging. Cell Metab. 2022;34:355–77.
34. Min J-Y, Chun K-S, Kim D-H. The versatile utility of cysteine as a target for cancer treatment. Front Oncol. 2023;12:997919.
35. Sbodio JI, Snyder SH, Paul BD. Regulators of the transsulfuration pathway. Br J Pharmacol. 2019;176:583–93.
36. Sánchez-Vega F, Gotea V, Margolin G, Elnitski L. Pan-cancer stratification of solid human epithelial tumors and cancer cell lines reveals commonalities and tissue-specific features of the CpG island methylator phenotype. Epigenetics Chromatin. 2015;8:14.
37. Hegde M, Joshi MB. Comprehensive analysis of regulation of DNA methyltransferase isoforms in human breast tumors. J Cancer Res Clin Oncol. 2021;147:937–71.
38. Telkoparan-Akillilar P, Panieri E, Cevik D, Suzen S, Saso L. Therapeutic targeting of the NRF2 Signaling Pathway in Cancer. Molecules. 2021;26:1417.
39. Harris IS, DeNicola GM. The Complex interplay between antioxidants and ROS in Cancer. Trends Cell Biol. 2020;30:440–51.
40. Saito R, Suzuki T, Hiramoto K, Asami S, Naganuma E, Suda H, et al. Characterizations of three major cysteine sensors of Keap1 in stress response. Mol Cell Biol T. 2016;36:271–84.
41. Shin D, Lee J, You JH, Kim D, Roh J-L. Dihydrolipoamide dehydrogenase regulates cystine deprivation-induced ferroptosis in head and neck cancer. Redox Biol. 2020;30:101418.
42. Cuadrado A. Structural and functional characterization of Nrf2 degradation by glycogen synthase kinase 3/β-TrCP. Free Radic Biol Med. 2015;88:147–57.
43. Mitsuishi Y, Taguchi K, Kawatani Y, Shibata T, Nukiwa T, Aburatani H, et al. Nrf2 redirects glucose and glutamine into anabolic pathways in metabolic reprogramming. Cancer Cell. 2012;22:66–79.
44. Shirozu K, Tokuda K, Marutani E, Lefer D, Wang R, Ichinose F. Cystathionine γ-Lyase deficiency protects mice from galactosamine/lipopolysaccharide-Induced acute liver failure. Antioxid Redox Signal Mary. 2014;20:204–16.
45. Moloney JN, Cotter TG. ROS signalling in the biology of cancer. Semin Cell Dev Biol. 2018;80:50–64.
46. Cheung EC, Vousden KH. The role of ROS in tumour development and progression. Nat Rev Cancer. 2022;22:280–97.
47. Prasad S, Gupta SC, Tyagi AK. Reactive oxygen species (ROS) and cancer: role of antioxidative nutraceuticals. Cancer Lett. 2017;387:95–105.
48. Banjac A, Perisic T, Sato H, Seiler A, Bannai S, Weiss N, et al. The cystine/cysteine cycle: a redox cycle regulating susceptibility versus resistance to cell death. Oncogene. 2008;27:1618–28.
49. Badgley MA, Kremer DM, Maurer HC, DelGiorno KE, Lee H-J, Purohit V, et al. Cysteine depletion induces pancreatic tumor ferroptosis in mice. Science. 2020;368:85–9.
50. Moon PD, Kim MHO, Oh HA, Nam SY, Han NARA, Jeong HJA, et al. Cysteine induces longitudinal bone growth in mice by upregulating IGF-I. Int J Mol Med. 2015;36:571–6.
51. Zhang C, Liu X, Jin S, Chen Y, Guo R. Ferroptosis in cancer therapy: a novel approach to reversing drug resistance. Mol Cancer. 2022;21:47.
52. Liu J, Xia X, Huang P, xCT. A critical molecule that links cancer metabolism to redox signaling. Mol Ther. 2020;28:2358–66.

Publisher's Note

Springer Nature remains neutral with regard to jurisdictional claims in published maps and institutional affiliations.